# Preparation and Electrocatalytic Hydrogen Evolution properties of Lignin-derived Cabon/Ni/NiO Composites

*Shiyi Jiang[1], Xuan Yu[1], Leiting Han[1], Dan Qiao[1], Zhengping Zhao[1,*], Jiahao Wang[2], Mingqiang Zhong[2]*

[1] Zhijiang College, Zhejiang University of Technology, Hangzhou 310014, P.R. China
[2] College of Materials Science and Engineering, Zhejiang University of Technology, Hangzhou 310014, P. R. China
[*]E-mail: sjzhaolei@163.com

In recent decades, the lignin has been numerously abandoned in agricultural and paper industries, which is urging us to find the new usage of it. And in theory, lignin is a kind of available material as carbon source because of its low cost, wide distribution and abundant carbon content. Therefore, researchers intend to make it a flesh porous carbon as new energy material. In this paper, lignin-derived porous carbon was prepared by self-assembly method and combined with Ni/NiO. Then the nanocomposites' structure and hydrogen evolution reaction were studied. The main research contents and results were as follows: Ni/NiO and lignin-drived porous carbon were combined by in-situ synthesis, and the morphology, composition, structure, and electrochemical performance were characterized. It was found that Ni and NiO were indeed absorbed on porous carbon as crystals. The composite's specific surface area measured by BET was 115.4 $m^2 \cdot g^{-1}$, while pore volume is 0.04 $cm^3 \cdot g^{-1}$. And hydrogen evolution hyperpotential of the composite electrode is 0.446V at 10 mA.

## 1. INTRODUCTION

Nowadays, a variety of convenient and efficient high-tech products have become an important part of People's Daily life. By the end of the 21st century, researchers predict, demand for energy could triple. As a result of people's overuse, the reserves of various resources continue to decline, and a series of environmental pollution problems one after another. Therefore, the development and utilization of sustainable new energy has become a common social focus of the century topic [1-2].

Hydrogen energy is a secondary energy source that can be obtained by electrolysis of water without worrying about its source [3]. It not only has good combustion performance, but also the product of the reaction is water, which has no impact on the environment. It is a clean and pollution-free energy. More specifically, hydrogen can be compressed and stored, which can be used as a backup fuel for some hydrogen fuel cells and has three times the energy density of conventional automobile fuel [4-6]. Therefore, developing hydrogen energy is the general trend.

The reaction that produces hydrogen gas is a hydrogen evolution reaction. It is a semi-reaction of water cracking to hydrogen and oxygen, in which hydrogen ions gain electrons at the cathode and are reduced to hydrogen. While in an alkaline medium, the water is directly reduced to hydrogen. Although the reaction produced by hydrogen is simple and only two electrons are involved, the energy barrier accumulated in the whole reaction is very high due to the multi-step elementary reaction mechanism. The theoretical decomposition voltage of water in thermodynamics is 1.23V. But due to the reason of overpotential, the load voltage of electrolytic tank needs 2~3 V in the actual test, which has a great influence on the overpotential of hydrogen [8]. The material with the best performance of hydrogen evolution is platinum electrode. Due to its small hydrogen overpotential, the voltage required for water electrolysis is relatively small, thus saving energy. However, platinum is a precious metal, which limits its commercial application in electrodes. Therefore, it is necessary to search for electrode materials with low overpotential and Tafel value like platinum.

In terms of hydrogen evolution performance, nickel as a transition metal and its oxides have become a hot research object due to its unique electronic structure [9-11]. On the other hand, the hydrogen evolution performance of the electrode can be further improved and the energy consumption can be reduced by optimizing the electrode structure and catalytic composition. This can be achieved by combining a number of precursors with a porous carbon that can be designed. Since both nickel and nickel oxide have been reported to catalyze the cracking of water, the combination of the two may have a synergistic effect to increase the catalytic efficiency.

Carbon is abundant in nature and is found in all organic matter. Carbon can be hybridized in a variety of ways, and when it bonds with different hybridized orbitals, not only can it form a variety of organic compounds, but it can also produce carbon-based materials with different shapes and different properties [12-14]. Among all kinds of carbon materials, porous carbon materials have numerous pores inside, leading to their large specific surface area and equally excellent electrical conductivity. The precursors prepared by porous carbon materials are generally organic matter, so their sources are wide and can be industrialized. They are widely used in energy storage and transformation, catalytic materials or adsorption materials. A variety of organics in nature can be used as the precursor of porous carbon and lignin is one of them. Lignin, a natural aromatic polymer, is second only to cellulose in the plant kingdom in content and abundance, accounting for about 20~30% of the solid mass of plants [15]. Unlike cellulose, the utilization rate of lignin still has a very large room for improvement. Agricultural production and paper industry will produce a large amount of lignin waste. At present, a small part of these waste will be used as fuel, tanning agent or adhesive and other low value-added products, and the rest can only be discarded in order to avoid a large amount of additional consumption of manpower, materials and time for post-processing [16].

In this paper, a carbon sphere of lignin loaded with nickel oxide as a catalyst for hydrogen evolution is studied. The carbonization of microspheres were prepared by precipitation of sodium lignosulfonate, and Ni/NiO composites were grown by hydrothermal method. The electrode materials for hydrogen evolution were prepared. The structure and electrochemical properties were studied.

## 2. EXPERIMENTAL SECTION

### 2.1 Preparation of lignin-based C/Ni/NiO composites

Using Tween-80 or Tween-60 as emulsifier to synthesize lignin carbon spheres. Pour 500mL isopropanol into a round-bottomed flask and put it into an ultrasound tank for ultrasound and stirring at 300W. In addition, 0.6g of sodium lignosulfonate was put into a 50mL beaker, 20mL of deionized water was added and stirred, 20 drops of tween-80 were added as emulsifier, and then put into an ultrasonic pool for ultrasonic uniformity to obtain lignin dispersion. All the dispersible was injected into the syringe, and the syringe was fixed on a double-channel micro syringe pump. The syringe pump was set to inject the dispersible into isopropyl alcohol at a speed of 20mL/h. After the injection, ultrasonic treatment was continued for 2h. The mixture was centrifuged, and the precipitates were dried in vacuum to obtain a brown-yellow solid. The dried product is ground with a mortar and put into a porcelain boat and calcined in a tubular furnace ($N_2$ atmosphere, 5°C/min to 1000°C, holding for 1h) to get black powder. The powder is poured into the mortar and ground again to get the finished carbon ball emulsified by Tween-80, which is recorded as LC80. By replacing Tween-80 with Tween-60 to repeat the above synthesis steps, the carbon sphere emulsified by Tween-60 was produced, which was denoted as LC60.

### 2.2 Ni/NiO recombination with carbon spheres

0.9g of prepared carbon balls were taken and divided into 3 parts according to each 0.3g. 0.5M, 1.0M and 1.5M $Ni(NO_3)_2$ solutions of 100ml each were mixed with three carbon spheres respectively. After ultrasonic treatment for 4h, they were loaded into a centrifuge tube for 8min to make the nickel fully attached to the carbon spheres. At the end of centrifugation, 0.8g NaOH was added to it to react with $Ni(NO_3)_2$ to form $Ni(OH)_2$. Adding 0.7 GnAbH4 makes part of Ni reduced. Finally, the supernatant was sufficiently centrifuged and poured out, and dried in a vacuum at 60 °C for 48h, then calcined in a tubular furnace at 500 °C for 6h. After cooling, the composite Ni/NiO carbon balls were obtained and ground into powder for testing. According to the concentration of $Ni(NO_3)_2$ used, the three composite microspheres prepared with Tween-80 were respectively recorded as LC80-N5, LC80-N10 and LC80-N15 from low to high, and accordingly, the three composite microspheres prepared with Tween-60 were respectively recorded as LC60-N5, LC60-N10 and LC60-N15.

*2.3 The mainly characterization and testing*

FT-IR spectra of all samples were recorded using polymer granule on a Perkin-Elmer Wellesley MA spectrophotometer. Thermogravimetric analysis (TGA) was performed on a TGA 7 instrument (PerkinElmer) thermal analysis system. Sample weight taken was 2-4 mg. All the experiment data were taken as an average of at least five measurements. The microstructures were observed on a Scanning Electron Microscope (Hitachi S4000, Japanese) and a Transmission Electron Microscope ( JEM-100CX II, Japanese). Raman spectroscopy is a method for qualitative analysis of molecular structure. The chemical structures were observed on a Lab RAM HR UV800 laser Raman spectrometer (JOBIN YVON, France). The excitation light source is 632.81 nm and the scanning range is 200~4000. The XPS (KRATOS AXIS Ultra DLD, Shimazu KRATOS) was used. The light source was AI-KaX rays and the vacuum degree was $3*10^{-7}$ Pa. Nitrogen adsorption test (BET) was using the automatic physical adsorption instrument (ASAP2020, mack instruments). X-ray diffractometer (X'pert PRO, PANalytical) was used. The test parameters of the instrument are as follows: 36 kV, 30 mA and Cu radiation.

The constant charge-discharge performance was tested after the sample electrode material was assembled into CR 2025 button battery. The electrochemical performances such as power density, energy density and specific capacitance can be obtained by processing and analyzing the results of constant current charge-discharge test [17]. The calculation formula of specific capacitance is:

$$Cs = I\Delta t/m\Delta V \tag{1-1}$$

Where I(A) is the charge-discharge current. $\Delta t$ for discharge time. m is the mass of the active substance in the electrode material. $\Delta V$ is the discharge voltage range.

The cyclic voltammetry is to discuss the reaction of capacitor electrode after applying triangular waveform potential. The applied control signal is potential, and the measured corresponding signal is current. It is mainly to study the change rules of I-t and I-U. The relation curve of U-I can be obtained by observing the T-t graph [18].

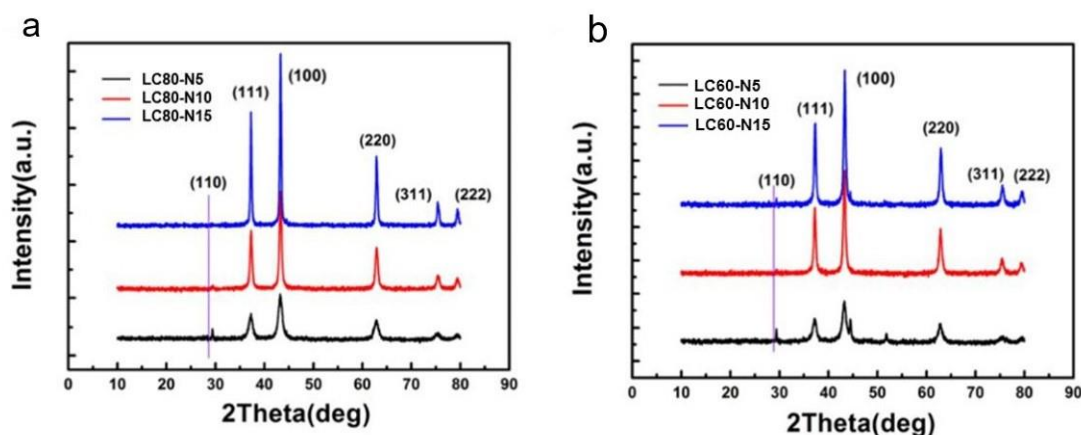## 3. RESULTS AND DISCUSSION



**Figure 1.** XRD spectrum of the lignin-derived C/Ni/NiO microspheres prepared by tween-80 (a) and tween-60 (b).

In order to confirm whether the synthesized composite microspheres have regular crystal structure, XRD analysis was performed first. Figure 1 (a) is the XRD pattern of C/Ni/NiO composite microspheres prepared by Tween-80. It can be seen that LC80-N5, LC80-N10 and LC80-N15 all have a sharp narrow peak at 2θ=44°, which is consistent with the characteristic peak representing the graphite-carbon (100) plane [20]. At 2θ=37.3°, 43.3° and 62.8°, these three peaks increase with the increase of Ni concentration ratio, representing the diffraction peaks of (111), (200) and (220) surfaces of NiO (JCPDS card number 47-1049). Ni at 2θ=44.5° should have a characteristic peak (JCPDS card number 45-1027) representing its (011) crystal plane. This peak cannot be clearly identified in the figure. This may be due to the excessive scanning rate, resulting in the overlap of three adjacent peaks of Ni at 2θ=44.5° and 43.3° and graphite carbon at 2θ=44°. Both LC80-N5 and LC80-N10 have a low peak at 2θ=29.5°, which is the characteristic peak of the (110) crystal plane of NIC. By burning at high temperatures, some of the Ni melts into the carbon shelf and bonds with C. However, with the increase of Ni concentration ratio, this peak tends to disappear. Figure 1 (b) is the XRD pattern of C/Ni/NiO composite microspheres prepared by Tween-60. In the figure, the characteristic peaks of (111), (200) and (220) surfaces representing NiO appear at 2θ=37.3°, 43.3° and 62.8° for LC60-N5, LC60-N10 and LC60-N15. With the increase of Ni concentration ratio, the characteristic peak of NiO becomes stronger. At 2θ=29.5°, the characteristic peak of (110) plane representing NIC can still be found [21]. At the 2θ=44.5° of LC60-N5 and LC60-N15, a strong and weak Ni 2θ=44.5° characteristic peak can be distinguished, which proves that Ni crystals still exist after prolonged moderate oxidation and calcination treatment.
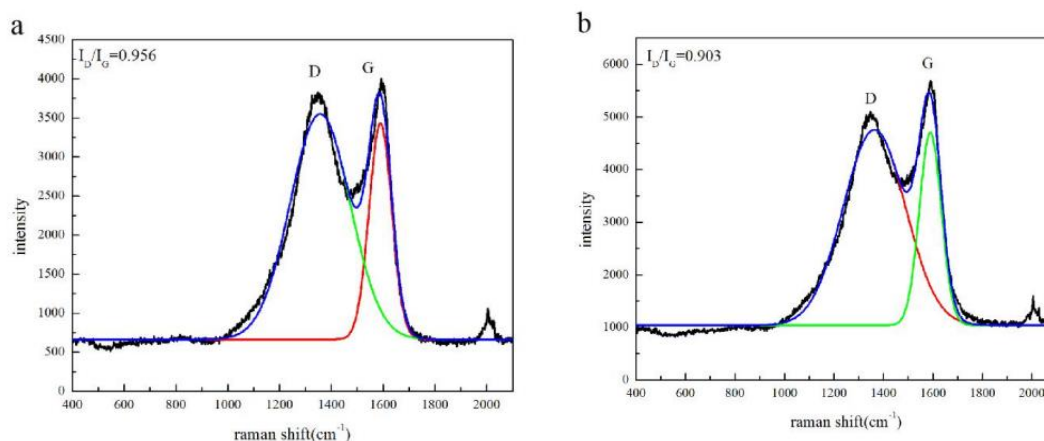


**Figure 2.** Raman spectrum of the lignin-derived carbon microspheres prepared bytween-80 (a) and tween-60 (b). The blue, green and red lines in the figure are computer fitting curves.

It is known from XRD pattern that the synthetic lignin-based carbon spheres have graphitized structure. In order to determine the effect of emulsifier on the graphitization degree of carbon spheres, the LC80 and LC60 were measured by Raman spectroscopy. In Figure 2, (a) represents LC80 and (b) represents LC60. The graphitization degree of the samples can be obtained by the ratio of the height of

D characteristic absorption peak at 1300 cm$^{-1}$ and the height of G characteristic absorption peak at 1600 cm$^{-1}$ on the abscess axis. The smaller the ratio, the higher the graphitization degree [22]. The results showed that D peak at 1317 cm$^{-1}$ and G peak at 1608 cm$^{-1}$ were observed for the two carbon globes, and the ID/IG ratio of LC80 and LC60 was 0.956 and 0.903, respectively. Both of them have higher graphitization degree, and the lignin-based carbon spheres prepared by adding Tween-60 are better than that of Tween-80.
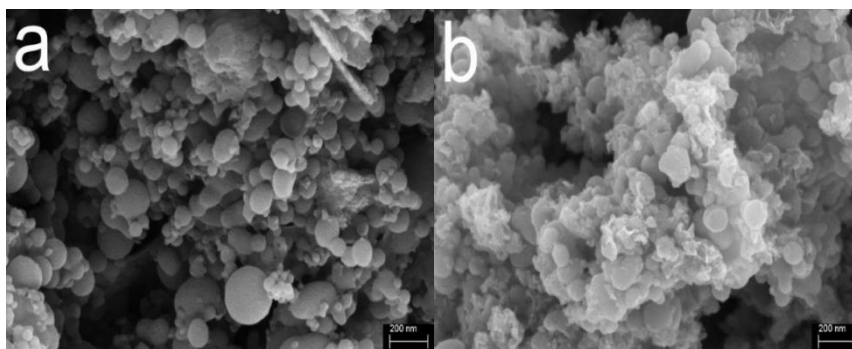


**Figure 3.** SEM images of the lignin-derived carbon (a) and the lignin-derived C/Ni/NiO microspheres prepared by tween-60 (b)

In order to determine the surface morphology and load condition of lignin carbon and its composites, scanning electron microscopy (SEM) was used to differentiate them. Fig. 3(a) shows LC60 of unloaded Ni/NiO. It can be seen from the figure that there are a lot of pores in the carbon material, but the distribution of carbon sphere diameter is not uniform. The reason may be that the mixing of sodium lignosulfonate with higher molecular weight makes the diameter of some carbon spheres larger. Figure 3 (b) shows LC60-N15 loaded with Ni/NiO. As can be seen from the figure, the microsphere surface is filled with tiny NiO or Ni crystals which presents with higher brightness in the gap. For the filling, the cavity is obviously reduced at the same rate.

Figure 4 is the TEM images of LC60-N15 at different resolutions. As can be seen from the figures, NiO or Ni crystals are formed on the surface of the carbon sphere, forming a sprouting shape with the carbon matrix. Among them, the spherical structure of carbon material is consistent with the SEM results, and the supported NiO or Ni crystals appear to agglomerate.

The diffraction pattern of the crystal, marked by a red arrow, is approximately 0.218 nm, 0.168 nm, and 0.238 nm wide. 0.218 nm corresponds to the (200) plane of NiO or the (002) plane of Ni. The 0.168 nm corresponds to the (220) plane of NiO and the 0.238 nm corresponds to the (111) plane of NiO or the (010) plane of Ni [23]. XRD results also prove the existence of diffraction peaks corresponding to these mirrors. Fig. 4(f) is the corresponding electron diffraction pattern, in which there are multiple diffraction points but no ring can be formed, which should represent that the crystal is polycrystalline and some of it tends to form single crystal.
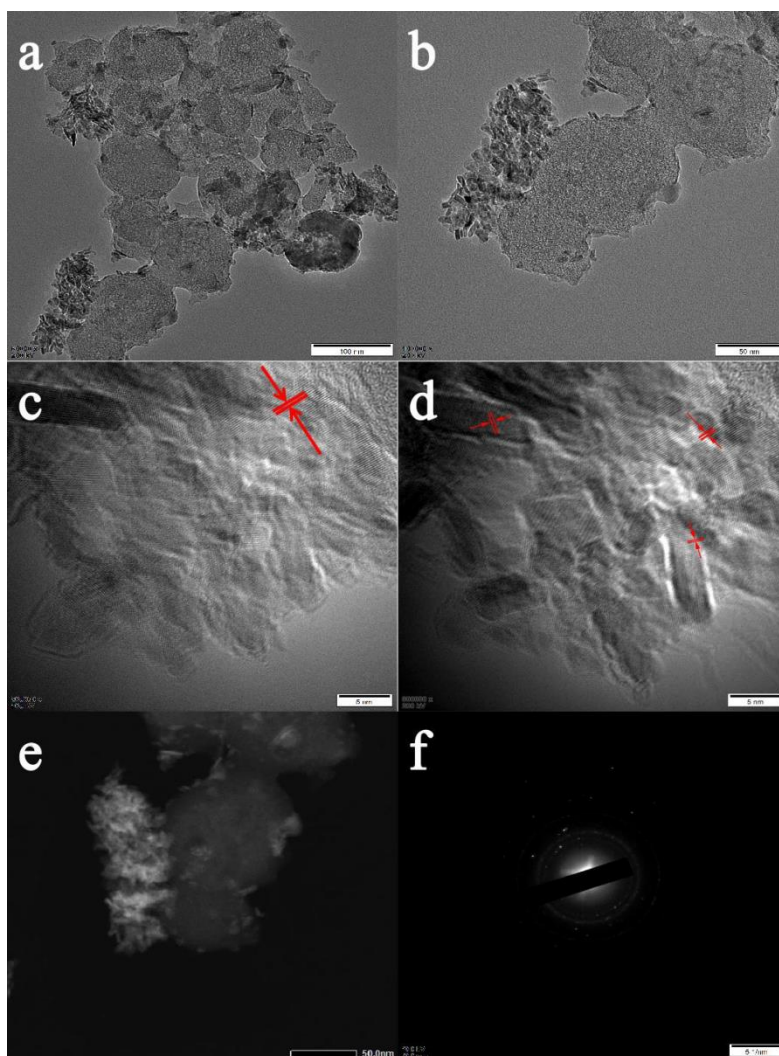
**Figure 4.** TEM images ofthe lignin-derived C/Ni/NiO microspheres LC60-N15 (a-e) and the corresponding electron diffraction pattern (f).


In order to observe the actual Ni/NiO load of LC80, EDS tests were performed on some TEM areas, as shown in Fig. 5. The brighter region in 5(a) is the region of nickel containing crystallization. The carbon spheres prepared with sodium lignosulfonate inevitably retain a partial skeleton bonded to oxygen, and in this crystallization region, the nickel signal is still more dense than the oxygen element, which should confirm the presence of not only NiO crystals but also many elemental Ni elements on the carbon spheres. By comparing the EDS signals of C and Ni elements, it can be found that there is little Ni in places with dense C signals, which indicates that the load of Ni is not so uniform. Where Ni signal is dense, there is also little C, which should only be the Ni and NiO crystal particles that hinder the detection of C signal.
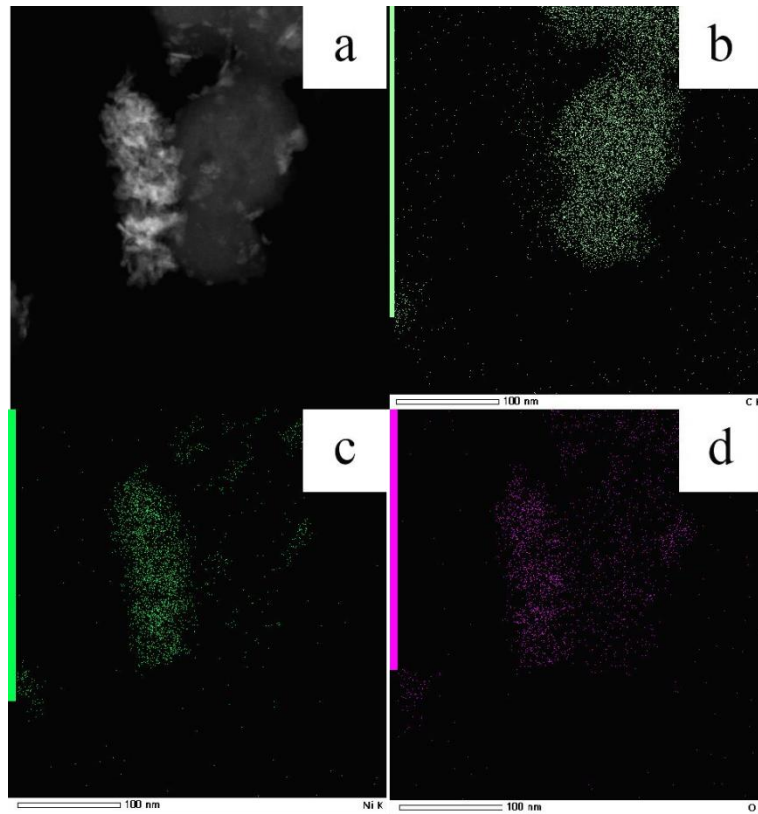
**Figure 5.** TEM image of the lignin-derived C/Ni/NiO microspheres LC80-N15 (a) and the corresponding elemental mapping of C (b), Ni (c) and O (d).
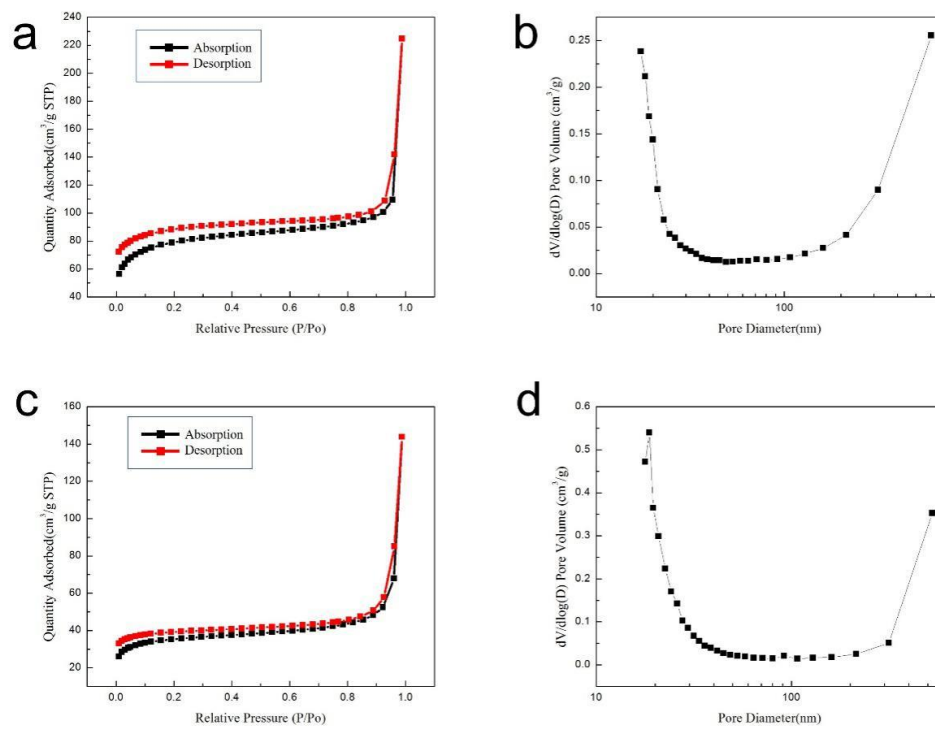


**Figure 6.** $N_2$ adsorption-desorption isotherms and pore size distribution of (a, b) the lignin-derived carbon microspheres LC80 and (c, d) lignin-derived C/Ni/NiO microsphere LC80-N15

BET tests were performed to test the specific surface area of the material as well as the pore size and distribution. Figure 6 (a) and (c) are the BET test results of LC80 and LC80-N15 respectively. The curves in the figure are all type IV isothermal curves of adsorption and desorption, and the adsorption amount gently increases at low pressure. At this time, $N_2$ molecules are adsorbed on the inner surface of the mesoporous from single layer to multi-layer. The hysteresis occurs during desorption, and the hysteresis line of LC60 never coincides with the adsorption curve, which may be caused by pore collapse. The hysteresis of Ni/NiO@LC60 forms a hysteresis loop, but the desorption rate is not affected during the hysteresis loop, indicating that the hysteresis loop is H3 type hysteresis loop, and the pores are slit pores formed by particle accumulation [24]. (b) and (c) are the corresponding pore size distribution diagrams, and the mesoporous amount of the two kinds of microspheres is less. BET test results show that the specific surface area of the unloaded and loaded nickel-carbon materials is 259.8 m$^2$/g and 115.4 m$^2$/g, respectively. It is mainly NiO and Ni that fill the pores to reduce the specific surface area of the microspheres. The pore volume of the carbon material without nickel loading is 0.08 cm$^3$/g, and the pore volume of the carbon material with nickel loading is 0.04 cm$^3$/g, which proves that NiO and Ni are loaded in the lignin-based carbon spheres.
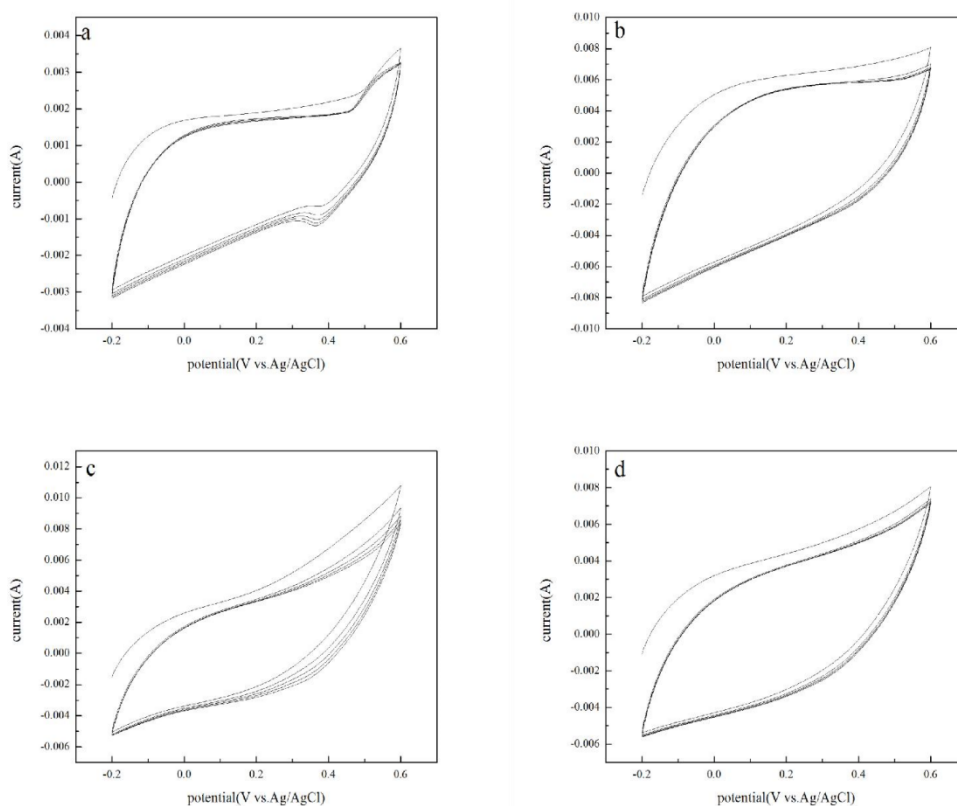


**Figure 7.** CV curves of the lignin-derived C/Ni/NiO microspheres prepared by (a, b) tween-60 or (c, d) tween-80 at different scan rates

The results of cyclic voltammetry test show that the CV curves of the two composite carbon spheres can maintain good repeatability and have a certain stability. The curve in Figure 7(a) has a REDOX peak in the range of 0.3-0.4V, indicating that REDOX reaction has occurred at the electrode.
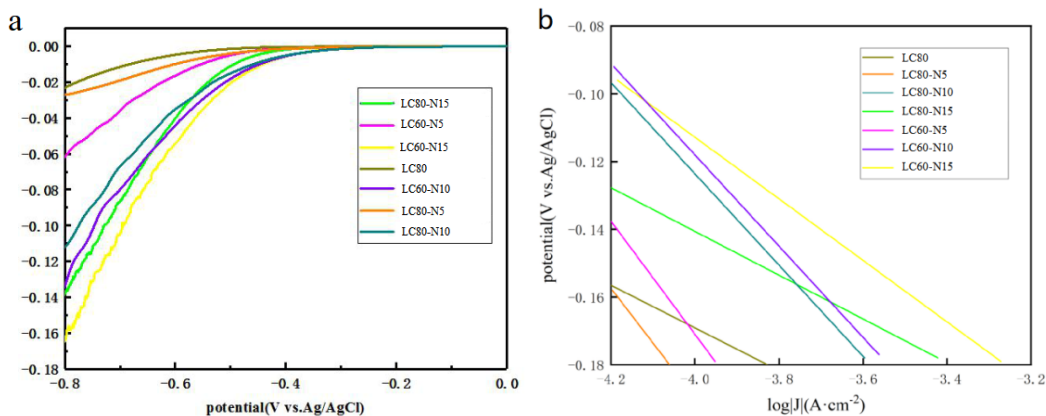
**Figure 8.** Polarization curves (a) and corresponding Tafel line of the lignin-derived C/Ni/NiO microsphere prepared with 0.5 M、1 M、1.5 M $Ni(NO_3)_2$ by tween-80 and tween-60 (b)

Figure 8 (a) shows the polarization curves of lignin-based carbon spheres LC80, LC80-N5, LC80-N10, LC80-N15, LC60-N5, LC60-N10 and LC60-N15 loaded with two emulsifiers (Tween-80 and Tween-60) and different concentrations of nickel nitrate (0, 0.5, 1, 1.5M). The potential is overpotential when the current is -0.01A. The maximum overpotential of pure carbon is 0.698 V. The overpotential of other electrodes is 0.611V, 0.559V, 0.497V, 0.468V, 0.457V and 0.446V, respectively, which is close to the HER overpotential of other electrode materials [25].

The hydrogen evolution activity parameters of different lignin-based carbon-nickel composites are listed in Table 3-1. It can be seen that the higher concentration of $Ni(NO_3)_2$, the better properties of the carbon materials treated. It is because that the more active substances are loaded, and the material properties treated with Tween-60 are better than those treated with Tween-80. Table 3-1 lists the calculated overpotential of LC80, LC80-N5, LC80-N10, LC80-N15, LC60-N5, LC60-N10 and LC60-N15 at 10mA and the corresponding Tafel slope. It can be seen that the higher Ni concentration ratio, the smaller Tafel slope is. The Tafel slope of the composite microspheres prepared by the two emulsifiers is very similar, while that of Tween-60 is generally higher.

**Table 1.** HER electrocatalytic performances of different lignin-derived C/Ni/NiO microsphere in 6M KOH

| Serial number | Overpotential （mV） | Tafel slope （mV·dec$^{-1}$） |
|---|---|---|
| LC80 | 698 | 63 |
| LC80-N5 | 611 | 162 |
| LC80-N10 | 468 | 134 |
| LC80-N15 | 497 | 66 |
| LC60-N5 | 559 | 167 |
| LC60-N10 | 457 | 135 |
| LC60-N15 | 446 | 91 |

## 4. CONCLUSIONS

In this chapter, lignin microspheres were formed by self-assembly with sodium lignosulfonate as raw material. The porous carbon materials were synthesized by calcination in Ar atmosphere at high temperature. Different concentrations of Ni were loaded onto the porous carbon spheres by in-situ synthesis method. After two times of calcination, NiO was generated and finally the lignin-based C/Ni/NiO porous composites were formed. XRD results show that there are a lot of Ni and NiO crystals in the composites. The crystal plane diffraction spacing measured by HRTEM also proves this point, and the NiO and Ni crystals exist in the form of polycrystalline with heterogeneous interfaces. Raman results show that the synthesized carbon material has a high graphitization degree. The BET results show that the porous carbon spheres have large specific surface area ($115.4 \sim 259.8$ $m^2 \cdot g^{-1}$) and contain mesoporous carbon spheres. SEM results show that the composite is spherical with porous structure, and the Ni and NiO are uniformly loaded on the spherical surface. According to the linear sweep voltammetry curve, the overpotential under 10 mA current is only 0.446 V, which is close to the best known hydrogen evolution performance. The properties of carbon composites supported by different concentrations of $Ni(NO_3)_2$ solution are different. The higher the concentration, the better performance of composite carbon materials. The properties of carbon materials prepared by dispersing sodium lignosulfonate with different dispersants are also different. The carbon material prepared by using Tween-60 as dispersant is better than that of Tween-80.

## References

1. S.M. Siddeeg. *Int. J. Electrochem. Sci.*, 15 (2020) 599.
2. L. Ma, X. Luo and A.J. Kropf. *Nano lett.*, 16 (2015) 781.
3. S.V. Gnedenkov, D.P. Opra, S.L. Sinebryukhov A.K. Tsvetnikov, A.Y. Ustinov and V.I. Sergienko. *J. Ind. Eng. Chem.*, 20 (2014) 903.
4. D.I. Choi, J.N. Lee, J. Song and D. Chew. *J. Solid State Electr.*, 17 (2013) 2471.
5. N. H. Attanayake and M. Tang. *Curr. Opin. Electrochem.*, 29 (2021) 100791.
6. M.M. Radhi, W.T. Tan, M.Z. Rahman and A.B. Kassim, *Int. J. Electrochem. Sci.*, 5 (2010) 254.
7. Y.L. Zhu, W. Zhou, Y. Zhong, Y.F. Bu, X.Y. Chen, Q. Zhong, M.L. Liu and Z.P. Shao. *Adv. Energy Mater.*, 7 (2017) 1602122.
8. D.M.F. Santos, C.A.C. Sequeira, D. Maccio, A. Saccone and J.I. Figueiredo. *Int. J. Hydrogen Energ.*, 38 (2013) 3137.
9. Z.W. Seh, Y. Sun, Q. Zhang and Y. Cui. *Chem. Soc. Rev.*, 45 (2016) 5605.
10. S.V. Gnedenkov, S.L. Sinebryukhov, D.P. Opra, L.A. Zemnukhova and V.I. Sergienko. *Procedia Chem.*, 11 (2014) 96.
11. W. Sun, Y.L. Zhang and F.Q. Yang. *Electrochimica Acta*, 367 (2021) 137573.
12. K. Babel, D. Janasiak and K. Jurewicz. *Carbon*, 50 (2012) 5017.
13. Z.L. Xu, J.K. Kim and K. Kang. *Nano Today*, 19 (2018) 84.

*Int. J. Electrochem. Sci.,* 16 **(2021)** Article Number: 211014

12

14. X. Liang, C.Y. Kwok, F. Lodi-Marzano, Q. Pang, M. Cuisinier, H. Huang, C.J. Hart, D. Houtarde, K. Kaup and H. Sommer. *Adv. Energy Mater.*, 6 (2016) 1501636.
15. Z. Li, H.B. Wu and X.W. Lou. *Energy Enviro. Sci.*, 9 (2016) 3061.
16. J. Schuster, G. He, B. Mandlmeier, T. Yim, K.T. Lee, T. Bein and L.F. Nazar. *Angew. Chem. Int. Ed. Engl.*, 51 (2012) 3591.
17. Z.P. Zhao, Z.P. Zhou, S.T. Shen and M.Q. Zhong, *Int. J. Electrochem. Sci.*, 10 (2015) 5880.
18. D.H. Kim, B. Lee, K.Y. Park and K. Kang. *Chem. Asian J.*, 11 (2016) 1288.
19. W.G. Chong, J.Q. Huang, Z.L. Xu, X. Qin, X. Wang and J.K. Kim. *Adv. Fun. Mater.*, 27 (2017) 1604815.
20. D. Lin, Y. Liu, A. Pei and C. Yi. *Nano Res.*, 10 (2017) 4003.
21. X.B. Cheng, R. Zhang, C.Z. Zhao and Q. Zhang. *Chem. Rev.,* 117 (2017) 10403.
22. L. Xiao, Y. Cao, J. Xiao, B. Schwenzer, M.H. Engelhard, L.V. Saraf, Z.Nie, G.J. Exarhos and J. Liu. *Adv. Mater.*, 24 (2012) 1176.
23. M. Li, Y. Bai, C. Zhang, Y. Song, S. Jiang, D. Grouset and M. Zhang. *Int. J. Hydrogen Energ.*, 44 (2019) 10677.
24. J. Zhang, Q. Zhang and X. Feng. *Adv. Mater.*, 31 (2019) 1808167.
25. L. Ma, X. Luo, A.J. Kropf, J. Wen, X. Wang, S. Lee, D.J. Myers, D.J. Miller, T. Wu and J. Lu. *Nano Lett.*, 16 (2016) 781.